System Identification and Tracking Control of a Flapping Wing Micro Air Vehicle

A Dissertation

by

SEUNGWAN RYU

Presented to the Faculty of the Graduate School of
Seoul National University
in Partial Fulfillment
of the Requirements
for the Degree of

MASTER OF SCIENCE

School of Mechanical & Aerospace Engineering

Seoul National University

Supervisor : Associate Professor H. Jin Kim

July 2015

to my

MOTHER, FATHER, and SISTERS

with love

Abstract

System Identification and Tracking Control of a Flapping Wing Micro Air Vehicle

Seungwan, Ryu
Department of Mechanical & Aerospace Engineering
The Graduate School
Seoul National University

The goal of system identification is to build mathematical models of dynamical systems that can be used in control techniques. This thesis is focused on identifying the dynamics of a flapping wing micro air vehicle (FWMAV) from measured flight data. Because of the nonlinear and complex dynamics and coupled variables of a FWMAV, discrete-time linear time-invariant (LTI) models for both the longitudinal and lateral dynamics which have dominant flight state variables are used as a basis for system identification. To gather input-output data sets from flight test, an experimental setup is constructed in an indoor environment using a motion capture system. Discrete-time LTI models are sought by employing linear estimator, support vector regression (SVR) and validated in the time domain flight data. The results show that SVR accurately produces the true FWMAV responses better than the linear estimator. After dynamic characteristics of a FWMAV are checked through matrix analysis, the obtained model is used to design feedback controllers for maintaining altitude. To verify the controller, a simulation is performed. Experimental results, using a FWMAV, of maintaining a flight altitude are also presented.

Keyword : System identification, Longitudinal and lateral dynamics, FWMAV, Linear estimator, SVR

Student Number : 2013-23067

Table of Contents

List of Figures

List of Tables

1

Introduction

Unmanned Aerial Vehicles (UAVs) had been developed with military purposes at the beginning. However, these days, various types of UAVs are used for civilian applications such as aerial photography, weather observation, disaster monitoring, distribution and communication, and application fields of the UAVs will be gradually expanded in the future.

A micro air vehicle (MAV), or micro aerial vehicle, is classified as UAVs that can be as small as 15cm in length, width or height defined by the US Defense Advanced Research Project Agency (DARPA). It is possible for them to fly in areas with limited accessibility due to their small size, which also makes them less likely to be detected. However, their low payload limits equipment of onboard sensors such as camera, GPS, accelerometer, gyroscope and so on. Besides, they are vulnerable to disturbance such as a strong wind. In general, MAVs can be categorized according to wing types such as a fixed wing, rotary wing and flapping wing, as exemplified in Fig 1.1.

A flapping wing micro air vehicle (FWMAV) is an aircraft that files by periodically flapping its wings generating lift and thrust force such as birds, bats and insects. Above all, inspired by biological systems, it has the advantage of being less noticeable, and makes up for weakness of a fixed-wing aircraft like as being impossible to hover and a rotary-wing aircraft such as having a loud noise and being easily influenced by ground effect.

For a long time, engineers have made distinguished accomplishments toward developing FW-

Figure 1.1: Examples of a fixed wing, rotary wing and FWMAV

MAV prototypes, studying on the effect of flapping wings on the flight and designing control algorithms for autonomous flight. Back, S. S., *et al* [1][2] developed a closed-loop altitude regulation for a FWMAV using custom made onboard electronics with an external camera and demonstrated autonomous flight control of a FWMAV capable of flying toward a target using onboard sensing and computation only. De Croon, *et al* [3][4] showed systematic approach in developing their FWMAVs such as the DelFly I, Del Fly II and DelFly Micro, and implemented on obstacle avoidance algorithm for the flapping wing DelFly II with two onboard stereo cameras. H. K. Jung, *et al* [5] developed new types of FWMAVs to carry more payloads. H. C. Park, *et al* [6] confirmed the effect of wing rotation angle change on force generation produced by flapping wings. Whitney, J. P, *et al* [7] conducted passive-rotation flapping experiments with insect-scale driven artificial wings to measure aerodynamic forces and three-degree-of-freedom kinematics. Hong D, *et al* [8] analyzed airfoil dynamics of FWMAV and developed mathematical model of flight attitude to apply a novel control method based on adaptive robust control. Sawyer, B. F, *et al* [9] demonstrated pitch angle control using the ocelli on a wire-mounted RoboBee that is a sub-100mg FWMAV and free to rotate about its pitch axis. Table 1.1 shows characteristics of FWMAVs about 2 types (insect and bird) under development around the world.

1.1 Literature review

System identification is statistical methods to build mathematical models of dynamical systems which can be as simple as a graph of the input-output response or as complex as a set of differential equations of motion from the measured response to specific control inputs. In this way, a high fidelity model can be got using proper data sets. This model might be desired to characterized the system as a whole or subsystem. Most of the studies are interested in estimate linear models to apply classic control techniques. But, some authors apply to finding robust model with nonlinear identification to design advanced control techniques. Ljung L. [10] provides a basic knowledge on system identification theory. Various identification methods have been especially developed to model fixed-wing and rotary-wing aircraft. Tischler, Mark B., *et al* [11] explains fundamental system identification methods and procedures to apply to fixed-wing and rotary-wing aircraft. Andrei, D., *et al* [12][13] provided a systematic procedure for modeling, and identifying the linear and nonlinear dynamics of fixd-wing UAVs using a frequency domain system identification method by means of the CIFER software package. D. Schafroth *et al* [14] identified the coaxial micro helicopter using measurement data as well as a nonlinear identification tool, the Covariance Matrix Adaptation Evolution Strategy (CMA-ES) and designed H_∞ controllers for attitude and heave control. Gregory, G., *et al* [15] presented the estimation of a linear model for the dynamics of a quadrotor micro air vehicle and provided valuable parameters of aerodynamic and speed stability derivatives for development of improved controllers and observers.

1.2 Thesis contribution

The contributions of this paper are the following: first, we construct a control experiment setup for a MAV in indoor environment using a motion capture system to gather input-output data sets from flight tests. Next, to obtain longitudinal and lateral dynamics, we accomplish system identification of a FWMAV through time domain techniques such as linear estimator and support vector regression. After that, we analyze each dynamic characteristic. Finally, the acquired model is used to design feedback controllers such as pole placement reference tracking controller and linear quadratic tracking controller for maintaining altitude in simulation and we perform the experiment to validate the overall approach.

Table 1.1: Characteristics of FWMAVs under development around the world

Property	Weight(g)	Wingspan(cm)	Wing #	Power
Harvard Microrobotic Fly	0.06	3	2	x
Fukuoka Institute of Tech.	2.3	10	4	o
Purdue Univ.	2.6	11.4	2	x
Carnegie Mellon Univ.	2.7	12	2	x
TU Delft MicroDelfly	3.1	10	4	o
CalTech Microbat	10.5	15	2	o
Univ. of Maryland Small Bird	12.8	33	2	o
Nano Hummingbird	19	16	2	o
TU Delft Delfly Explorer	20	28	4	o
UC Berkeley Biomimetic Lab	13	26	4	o
Georgia Tech Robot Dragonfly	25	15	4	o

1.3 Thesis outline

The rest of this paper is organized as follows. In Chapter 2, an experimental setup and different kinds of the FWMAVs are described. In Chapter 3, an orientation of the FWMAV and system identification methods are presented in detail. In Chapter 4, system identification results of longitudinal and lateral dynamics are provided. In Chapter 5, a linear control framework is explained. Simulation and experimental results are provided in Chapter 6. Concluding remarks and potential future work are included in Chapter 7.

2

Experimental setup overview

Two FWMAVs are compared and shown in Fig 2.1. Geometric and physical specifications of the platforms are listed in Table 2.1.

Model-1 has one pair of flapping wings and Model-2 has two pairs of flapping wings. The maximum speed of Model-1 is approximately 4m/s and model-2 is about 2.5m/s. In addition, the pitch motion of Model-1 shakes more than Model-2 in flight. It means that Model-1 is vulnerable to some disturbances resulted from flapping wing motions. Therefore, Model-2 is appropriate for flight in limited indoor environment.

The FWMAV used in this paper has conventional two pairs of flapping wings with rudder and elevator control surfaces. The propulsion system is composed of an electric DC motor that drives two pairs of flapping wings with the same stroke plane. It is configured with an inverted T tail and the rudder control surface is actuated by electric coil with maximum deflection limits of 45 degrees in each direction which limited the control policy to be bang-off-bang control. The elevator control surfaces which are not used in this experiment are manually operated before the initiation of the flight.

Vicon motion capture system, an indoor GPS system, is used to measure the attitude and position of the FWMAV. With this system, the measured attitude and position are computed up to 100Hz through 3 markers that are placed on its fixed structure. For example, one is attached to the front of the head and the others are attached to the horizontal tail plane. The 8 vicon cameras are installed in an indoor room capturing a volume of 5m long, 4m wide and 2m height.

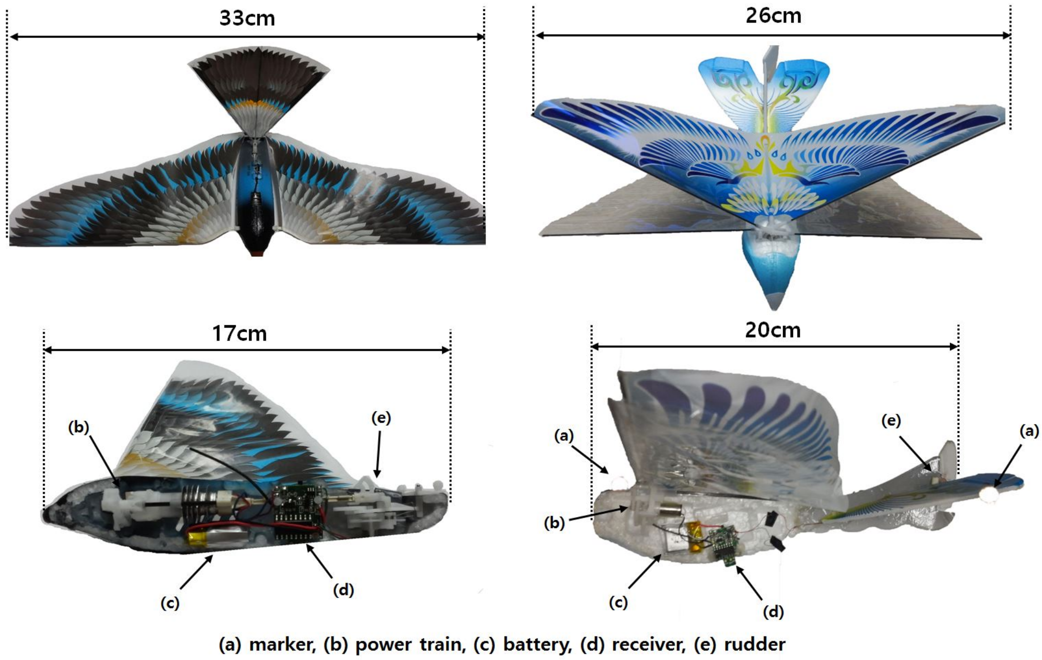

Figure 2.1: Components of the two FWMAVs used in the flight test. Model-1 (left) and Model-2 (right)

Table 2.1: Specifications of the two FWMAVs

Property	Model-1	Model-2	Units
Weight	8.85	14	g
Length	17	20	cm
Wing span	33	27	cm
Wing angle	55	45	degree
Flapping speed	18	19	flaps/sec
Max speed	3.5	2.5	m/s
Battery	55	70	mAh

To transmit the control signal to the FWMAV, a general 2 channel (one is flapping DC motor and the other is rudder control) remote control (RC) transmitter is connected to a control module which consists of Arduino and a motor driver at ground station. The type of output voltage of Arduino is generally a pulse width modulation (PWM) signal. Therefore, the motor driver is used to convert a PWM signal into a constant signal because the transmitter is operated by constant voltage between 0 and 3.4V.

Fig. 2.2 shows the overall automatic control system. When the user programmes certain input signals used to system identification at Arduino, the control module converts the input signals into the voltage signals to operate the transmitter. Then, the radio signals generated from the transmitter is sent by radio communication to the target FWMAV. The platform then fly according to the control signal in vicon volume. After that, the vicon computer save flight data consisting of position (x, y, z) and attitude (ϕ, θ, ψ)

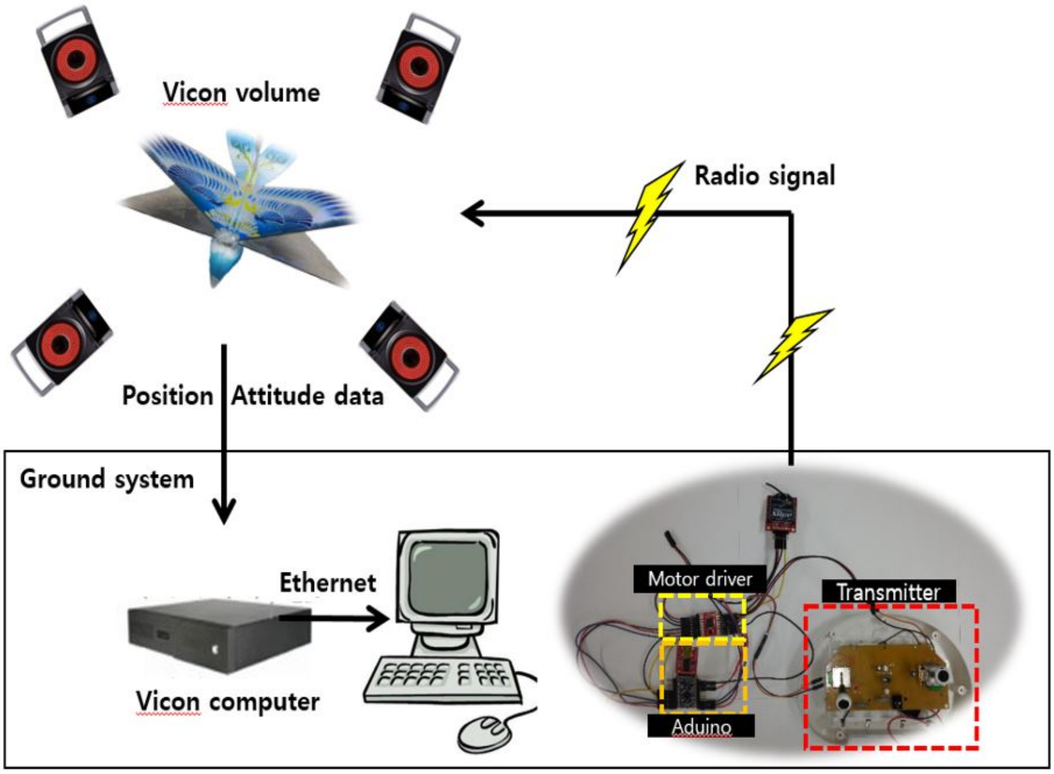

Figure 2.2: Overview of the automatic control system used for system identification

3

System identification

This chapter is organized as follows; Section 3.1 explains a detailed reference coordinates of the FWMAV. Section 3.2 introduces linearization of longitudinal dynamics and lateral dynamics. Section 3.3 presents input signal design for the identification of the FWMAV. Section 3.4 and Section 3.5 explain an overview of the theoretical background to system identification methodology (linear estimator and support vector regression).

3.1 Reference coordinates

We consider estimating the FWMAV's states during the flight tests. The coordinates of the 3 markers were transformed from reference frame (X_i, Y_i, Z_i) of the vicon volume to body frame (X_b, Y_b, Z_b) of the FWMAV, as showed in Fig. 3.1. The unit vectors of the body frame and the reference frame are related to the respective entries of the 3-2-1 rotation matrix sequence described in (3.1) which is one of the most widely used parameterisations. Before proceeding further, let us use the shorthand notation $S_\psi \equiv \sin\psi$, $C_\psi \equiv \cos\psi$, $S_\phi \equiv \sin\phi$, $C_\phi \equiv \cos\phi$, and so forth.

$$R_{bi} = \begin{bmatrix} C_\theta C_\psi & -C_\theta S_\psi & S_\theta \\ C_\psi S_\phi S_\theta + C_\phi S_\psi & C_\phi C_\psi - S_\phi S_\theta S_\psi & -C_\theta S_\phi \\ -C_\phi C_\psi S_\theta + S_\phi S_\psi & C_\psi S_\phi + C_\phi S_\theta S_\psi & C_\phi C_\theta \end{bmatrix} \tag{3.1}$$

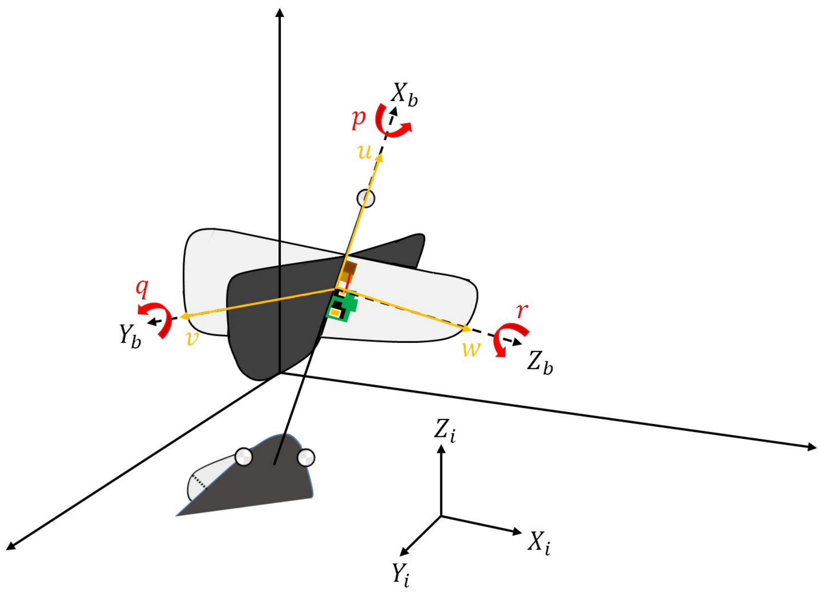

Figure 3.1: Configuration of the inertial $(X_iY_iZ_i)$ and body $(X_bY_bZ_b)$ coordinates for the FWMAV

We can determine the absolute velocity $(\dot{x}, \dot{y}, \dot{z})$ and the Euler rates $(\dot{\phi}, \dot{\theta}, \dot{\psi})$ by differentiating the positions and the Euler angles of center of gravity of the FWMAV with respect to time using 1^{st} derivative centered-difference.

The relationship between the angular velocities in the body frame (p, q, r) and the Euler rates also can be determined from (3.2)

$$\begin{bmatrix} p \\ q \\ r \end{bmatrix} = \begin{bmatrix} 1 & 0 & -S_\theta \\ 0 & C_\phi & C_\theta S_\phi \\ 0 & -S_\phi & C_\theta C_\phi \end{bmatrix} \begin{bmatrix} \dot{\phi} \\ \dot{\theta} \\ \dot{\psi} \end{bmatrix} \tag{3.2}$$

The total 15 states are recalculated: velocity in inertial coordinate $\overrightarrow{V_i} = (\dot{x}, \dot{y}, \dot{z})$; velocity in body coordinate $\overrightarrow{V_b} = (u, v, w)$; Euler angles (ϕ, θ, ψ); Euler rates $(\dot{\phi}, \dot{\theta}, \dot{\psi})$ and angular velocities $\overrightarrow{w} = (p, q, r)$.

3.2 Linearization of longitudinal dynamics and lateral dynamics

It is widely known that the FWMAV is a very complicated system for identification due to its time-varying and highly nonlinear. Some simplifying two assumptions will reduce the complexity of the problem. First, if we focus on small deviations about a steady flight condition, the nonlinear dynamics can be approximated with linear models. In this work, discrete time LTI model is chosen and we assume that the FWMAV is flying in a steady flight condition and that the excitations around trim condition are small. Second, we should assume that the motion of the FWMAV can be analyzed by dividing the equations into two groups. To separate the equations, the longitudinal and lateral equations must not be coupled. Under these assumptions, the modelling approach is valid if the FWMAV is not undergoing a large amplitude or very rapid maneuver.

Discrete-time LTI models of flight dynamics is linearized at the following operation point. This operation point represents the straight steady flight condition desired for the FWMAV.

$$x_0^{Lon} = [0.4836 \quad -0.7058 \quad 0.9705 \quad 0]^T, \;\; u_0^{Lon} = [225]$$

$$x_0^{Lat} = [0 \quad 0 \quad 0 \quad 0]^T, \;\; u_0^{Lat} = [0]$$

By applying small deviation theory, the following equations are derived. The matrix G is referred to as the system matrix where G is a known 4×4 matrix and the matrix H is the input matrix where H is a known 4×1 matrix

$$\begin{aligned} \Delta x_{k+1} &= x_{k+1} - x_0 \\ \Delta u_{k+1}^T &= u_{k+1}^T - u_0 \\ \Delta x_{k+1} &= G\Delta x_k + H\Delta u_k^T \end{aligned}$$

where

$$\begin{aligned} \Delta x_k^{Lon} &= [\Delta u_k \quad \Delta w_k \quad \Delta\theta_k \quad \Delta q_k]^T, \quad \Delta u_k^{Lon} = \Delta\delta_k^f \\ \Delta x_k^{Lat} &= [\Delta v_k \quad \Delta p_k \quad \Delta r_k \quad \Delta\phi_k]^T, \quad \Delta u_k^{Lat} = \Delta\delta_k^r \end{aligned}$$

3.3 Input signal design

An input design that excites the dynamic responses of the FWMAV is essential to assure the quality of the dynamic responses. In the time domain, the inputs that are commonly used for flight-test maneuvers for identification purposes are chirp input, step input, doublet input and multi-step.

Chirp input is a signal in which the frequency increases ('up-chirp') or decreases ('down-chirp') with time. In some sources, the term chirp is used interchangeably with sweep signal. Step input is a signal which has a maximum deflection of the control surface toward one direction for the specific time. Doublet input consists of a maximum defection of the control surface toward one direction during the specific time followed by a maximum deflection toward opposite direction. Fig 3.2 shows some maneuver inputs used for system identification.

The confined flight space and rapid reactivity of the FWMAV limited the test input selection. In longitudinal dynamics case, the input signal which effects on the motor of flapping part is made from several sine commands. On the other hand, nothing signal passes to the rudder. It means that the rudder is fixed in flight. In lateral dynamics case, the input signal which operates on the actuator of rudder part consists of doublet commands. On the other hand, the constant input to maintain altitude applies to the flapping motor in flight. Fig 3.3 shows some maneuver inputs used for experiment.

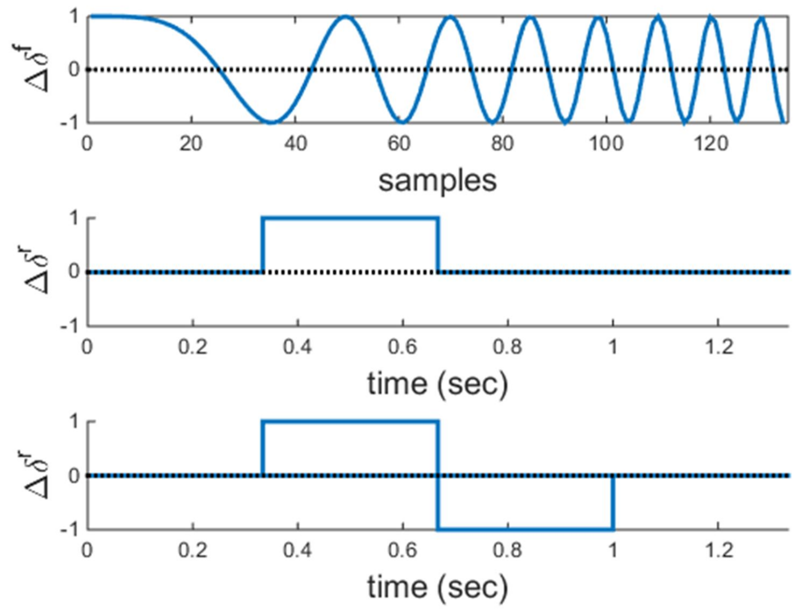

Figure 3.2: Example of maneuver input forms for system identification. Chirp signal (top), Step signal (middel) and doublet signal (down)

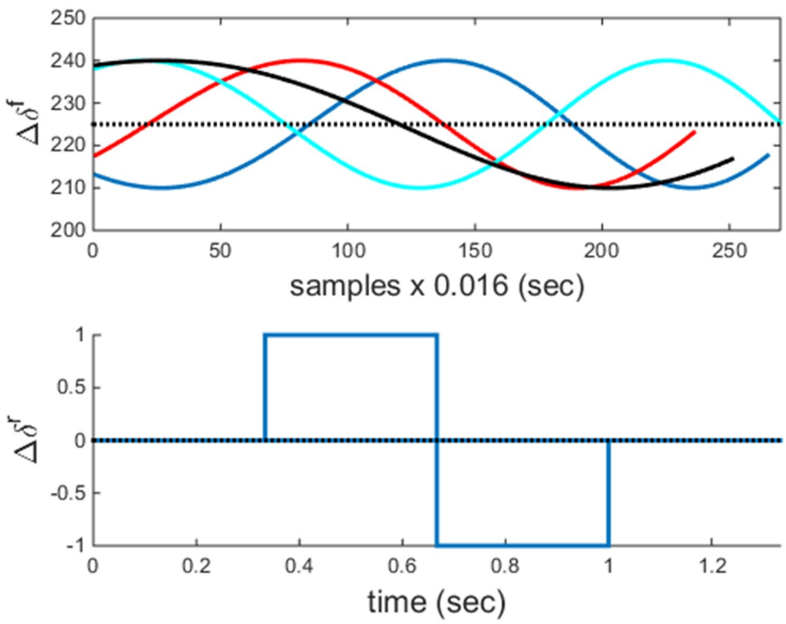

Figure 3.3: Maneuver input forms used in the experiment

3.4 Linear estimator

A linear estimator is designed to estimate the system matrix and the input matrix in the longitudinal and lateral dynamics. As am example, although we represent the longitudinal dynamics case, the lateral dynamics case is also represented in the same way, to estimate the $G \in R^{4\times4}$ and $H \in R^{4\times1}$ matrix in (3.3) we get:

$$\Delta x_{k+1}^{Lon} = G^{Lon}\Delta x_k + H^{Lon}\Delta u_k^T$$

$$\begin{bmatrix} \Delta u \\ \Delta w \\ \Delta q \\ \Delta\theta \end{bmatrix}_{k+1} = \begin{bmatrix} G^{Lon} & H^{Lon} \end{bmatrix} \begin{bmatrix} \Delta u \\ \Delta w \\ \Delta q \\ \Delta\theta \\ \Delta\delta^f \end{bmatrix}_k \tag{3.3}$$

$$\begin{bmatrix} G^{Lon} & H^{Lon} \end{bmatrix} = \mathbf{\Phi}\mathbf{\Psi}^T(\mathbf{\Psi}\mathbf{\Psi}^T)^{-1} \tag{3.4}$$

with

$$\begin{aligned} \Delta\eta_k &= [\Delta u \;\; \Delta w \;\; \Delta q \;\; \Delta\theta \;\; \Delta\delta^f]_k^T \\ \mathbf{\Phi} &= [\Delta x_1^{Lon} \;\; \Delta x_2^{Lon} \;\; \ldots \;\; \Delta x_{k-1}^{Lon} \;\; \Delta x_k^{Lon}] \\ \mathbf{\Psi} &= [\Delta\eta_0 \;\; \Delta\eta_1 \;\; \ldots \;\; \Delta\eta_{k-2} \;\; \Delta\eta_{k-1}] \end{aligned}$$

Because the $\mathbf{\Psi}$ is full row rank and $\mathbf{\Psi}\mathbf{\Psi}^T$ is not singular, then $\mathbf{\Psi}^T(\mathbf{\Psi}\mathbf{\Psi}^T)^{-1}$ is right inverse of the $\mathbf{\Psi}$, in the sense that $\mathbf{\Psi}\mathbf{\Psi}^T(\mathbf{\Psi}\mathbf{\Psi}^T)^{-1} = I$. This estimator is optimal for linear models.

3.5 Support vector regression

In machine learning, support vector machines (SVM) are supervised learning models with associated learning algorithms that analyze data and recognize patterns. There are two main categories for support vector machines: support vector classification (SVC) and support vector regression (SVR). The purpose of SVR is to find a function $F(X_k)$ that has ϵ deviation from the real obtained data Y_i for all the training data. That is to say, we don't consider errors as long as they are less than ϵ and will not accept any deviation larger than than this [16].

We simply review the ε-SVR algorithm [17]. Suppose we are given training data set $D = \{X_k, Y_k\}_{k=1}^{M}$, where X_k is the k-th input data in the space Γ of the input and Y_k is the corresponding output value. The case of a function $F(X_k)$ which approximates the relationship between the input and output data has been described in the form as

$$F(X_k) =< W, \Phi(X_k) > +b \tag{3.5}$$

where W is a vector in the feature space $\aleph$, $\Phi(X_k)$ is a mapping from the input space to the feature space $\aleph$, $< .,. >$ denotes the dot product in Γ and b is the bias term. Hence we can write this problem as a convex optimization problem:

$$\begin{aligned} \text{minimize} \quad & \frac{1}{2}\|W\|^2 \\ \text{subject to} \quad & |Y_i - F(X_i)| \leq \varepsilon \end{aligned} \tag{3.6}$$

The above convex optimization problem is practicable in cases where $F(X)$ exactly exists and approximates all pairs (X_i, Y_i) with ε precision. one can introduce slack variables ξ_i, ξ_i^* to cope with infeasible constraints of the optimization problem (3.6), the formulation becomes

$$\text{minimize} \quad \frac{1}{2}\|W\|^2 + C\sum_{i=1}^{M}(\xi_i + \xi_i^*) \tag{3.7}$$

$$\text{subject to} \begin{cases} Y_i - < W, \Phi(X_i) > -b \leq \varepsilon + \xi_i \\ < W, \Phi(X_i) > +b - Y_i \leq \varepsilon + \xi_i^* \\ \xi_i, \xi_i^* \geq 0 \end{cases}$$

The constant $C > 0$ determines the trade-off between the $F(X)$ and the amount up to which deviations larger than ε are tolerated. The ε-intensive loss function described by

$$|\xi|_{\varepsilon} = \begin{cases} 0 & \text{if } |\xi| < \varepsilon \\ |\xi| - \varepsilon & otherwise \end{cases} \tag{3.8}$$

The dual form of (3.7) becomes a quadratic programming (QP) problem as follows

$$\min_{\gamma,\gamma^*} D_{\varepsilon} = \min_{\gamma,\gamma^*} \Big[\frac{1}{2}\sum_{i=1}^{M}\sum_{j=1}^{M} K(X_i, X_j)(\gamma_i - \gamma_i^*)(\gamma_j - \gamma_j^*) + \varepsilon \sum_{i=1}^{M}(\gamma_j + \gamma_j^*) - \sum_{i=1}^{M} Y_i(\gamma_j - \gamma_j^*)\Big] \tag{3.9}$$

$$\text{subject to} \quad 0 \leq \gamma_i, \;\; \gamma_i^* \leq C, \;\; \sum_{i=1}^{M}(\gamma_i - \gamma_i^*) = 0, \;\; i = 1, \ldots, M \tag{3.10}$$

where $K(X_i, X_j)$ is a kernel function which has been defied as a linear dot product of the nonlinear mapping, i.e., $K(X_i, X_j) = \Phi(X_i)^T \Phi(X_j)$. Then, the one obtains $W = \sum_{i=1}^{M}(\gamma_j - \gamma_j^*)\Phi(X_i)$. When the support vectors corresponding to non-zero values of $\alpha_i = (\gamma_j - \gamma_j^*)$ are considered, (3.5) is modified

$$F(X_k) = \sum_{i=1}^{\#} \alpha_i K(X_k, X_i) + b \tag{3.11}$$

where # means the number of support vectors in the model [18].

The FWMAV model is identified offline method using input-output data sets. The nominal dynamic system is simply described by

$$x_{k+1} = f(x_k, u_k) = G(x_k) + H(x_k)u_k \tag{3.12}$$

where $x_k \in R^{N_x}$ means the state variables and $u_k \in R^{N_u}$ is the control input at time step k. The model of FWMAV is trained through the input-output data sets of (3.12). Each SVR is constructed for all state variables, so total of N_x SVRs are designed. The training set for the SVR is constructed as $D = \{X_i, Y_i^m\}$, where $i = 1, 2, \ldots, M$, M is the length of the training data, and $m = 1, 2, \ldots, N_x$. The superscript m means the m-th SVR. The $X_i (= [x_i, u_i])$ is the input of the SVR of FWMAV and $Y_i^m (= x_{i+1,m})$ is the corresponding output representing the m-th element of x_{i+1}. Thus, the output of the m-th SVR is represented by

$$\hat{Y}_k^m = \sum_{l=1}^{SV^m} \alpha_l^m K(X_k, X_l^m) + b^m \tag{3.13}$$

where SV^m is the number of support vectors of the m-th plant SVR.

4

System identification results

This chapter is organized as follows; Section 4.1 explains system identification results of longitudinal dynamics of the FWMAV. Section 4.2 presents system identification results of lateral dynamics of the FWMAV. Section 4.3 shows comparison results of linear estimator and SVR. For error minimization in system identification techniques, all data are filtered by zero-phase filters to minimize start-up and ending transients, and filter out high frequency noise. The flight test data are divided into identification and validation sets. The identification sets are used to estimate the system matrix and the input matrix, and the validation set is used to verify whether estimated model is able to represent state variables before it can be used for control design.

4.1 Longitudinal dynamics

The length of identification data used to estimate the models is 4×2156 and validation data used to verify the models is 4×269

Fig 4.1 shows results of the identified model of longitudinal dynamics with a input signal which consists of two pick values and one low value during time history. The blue line is real flight data, the red dash line is estimated data from identified model and the black dash line refers to trim value at each graph. Although there are some delays and errors between real data and identified data, the obtained model of the flight dynamics closely estimates the true FWMAV response.

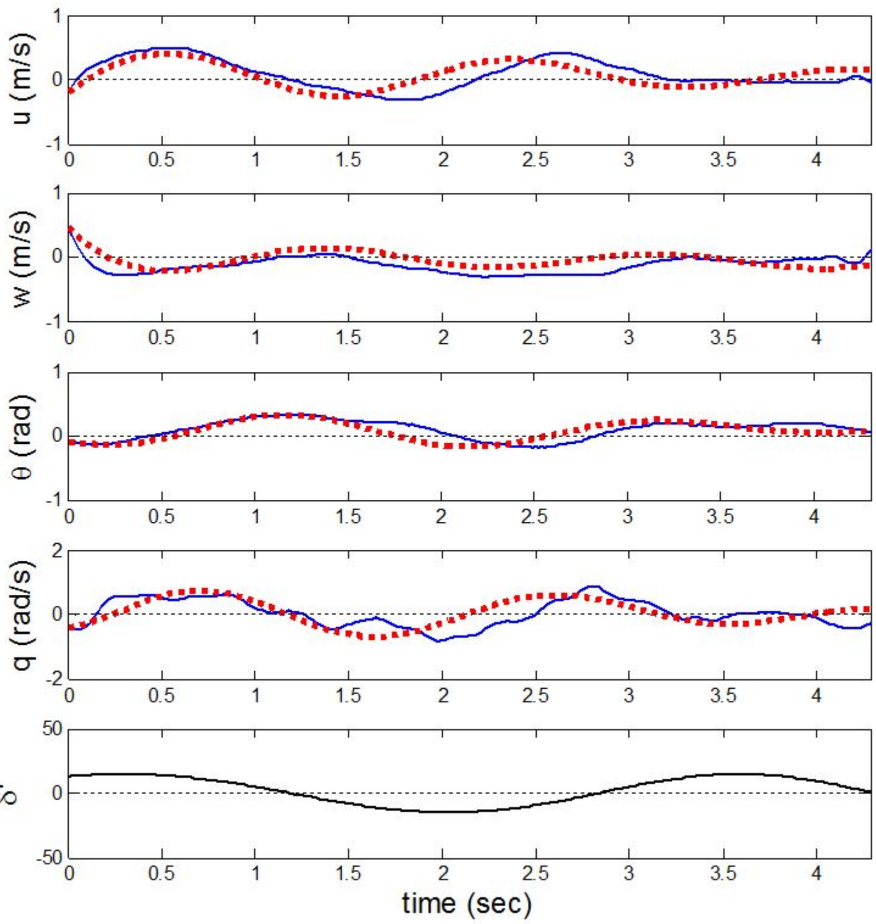

Figure 4.1: Time domain validation results of the longitudinal dynamics

$$\Delta x_{k+1}^{Lon} = G^{Lon}\Delta x_k + H^{Lon}\Delta u_k^T \tag{4.1}$$

$$G^{Lon} = \begin{bmatrix} 0.9908 & 0.0099 & -0.0705 & -0.0157 \\ 0.0123 & 0.9570 & 0.0638 & 0.0055 \\ -0.0008 & 0.0046 & 0.9957 & 0.0185 \\ 0.0335 & -0.0272 & -0.1178 & 0.9763 \end{bmatrix}, \quad H^{Lon} = \begin{bmatrix} 0.03882 \\ -0.04754 \\ 0.00350 \\ 0.03850 \end{bmatrix}$$

$$\Delta \dot{x}^{Lon} = A^{Lon}\Delta x + B^{Lon}\Delta u^T \tag{4.2}$$

$$A^{Lon} = \begin{bmatrix} -0.566 & 0.6328 & -4.512 & -0.9591 \\ 0.7873 & -2.7564 & 4.1320 & 0.3223 \\ -0.0746 & 0.3127 & -0.2127 & 1.1733 \\ 2.1347 & -1.7497 & -7.3274 & -1.4064 \end{bmatrix}, \quad B^{Lon} = \begin{bmatrix} 0.0248 \\ -0.0307 \\ 0.0021 \\ 0.0236 \end{bmatrix}$$

Table 4.1: Details of the longitudinal dynamics

Discrete-time eigenvalue	Continuous-time eigenvalue	Damping	Frequency
0.9951+0.0547i	-0.2123 + 3.4298i	0.0618	3.44
0.9951 - 0.0547i	-0.2123 - 3.4298i	0.0618	3.44
0.9404	-3.8418	1	0.675
0.9893	-0.6751	1	3.84

Using linear estimator expressed by (3.4), the system and control matrix in the longitudinal model can be approximated. The resulting of discrete time model is summarized by the matrices in (4.1) and continuous model converted from the obtained discrete model is also described by the matrices in (4.2).

Eigenvalue decomposition of the system matrix A^{Lon} reveals the modes of longitudinal dynamics. In general, longitudinal motion of an fixed-wing aircraft disturbed from its equilibrium flight condition is characterized by two oscillatory modes. Its means is equal to having two pairs of complex conjugate poles. We see that one mode is lightly damped and has a long period. This motion is called the long-period or phugoid mode. The second basic motion is heavily damped and has a very short period; it is called the short-period mode. On the other hand, longitudinal motion of the FWMAV has a pair of complex conjugate poles $-0.0212 \pm 3.43i$ with a damping ratio of 0.0618 and natural frequency of 3.44rad/s. These poles are similar to the phugoid mode of a fixed-wing aircraft. The rest of two poles have strictly negative real parts at 0.675 and 3.84 rad/s. The controllability matrix $P = [B \quad AB \quad A^2B \quad A^3B]^{Lon}$ has rank 4. So the linear time-invariant system is controllable. The details of longitudinal dynamics are summarized in Table 4.1. Figure 4.2 also shows pole-zero map and bode diagram of longitudinal dynamics.

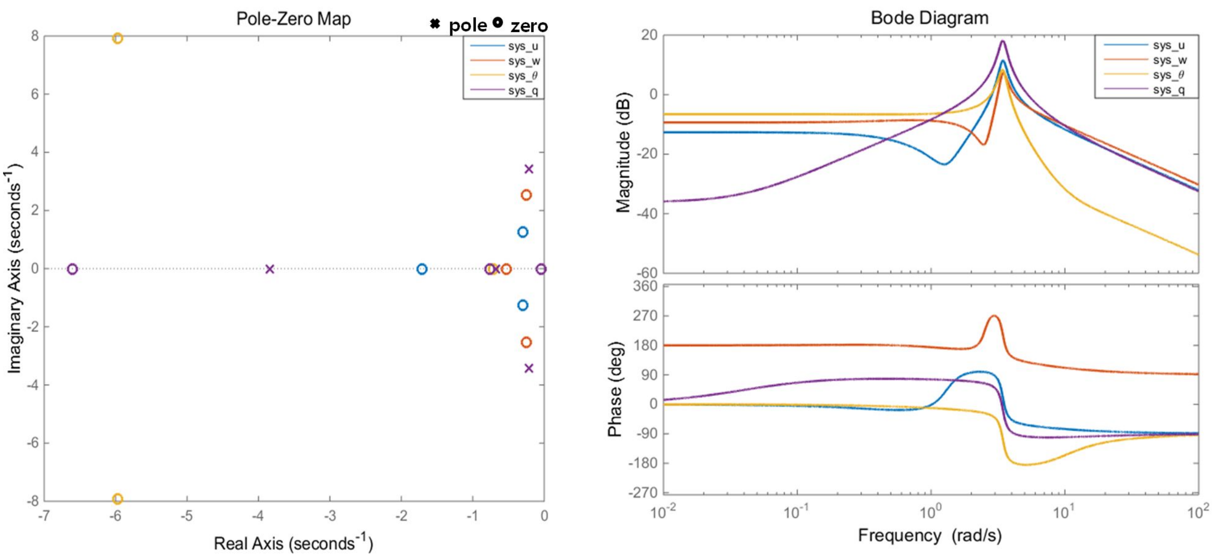

Figure 4.2: Pole-zero map and bode diagram of longitudinal dynamics

4.2 Lateral dynamics

The length of identification data used to estimate the models is 4×1615 and validation data used to verify the models is 4×185

Fig. 4.4 shows results of identified model of lateral dynamics of the FWMAV with a input signal which has single doublet input during time history. The blue line is real flight data, the red dash line is estimated data from identified model and the black dash line refers to trim value at each graph. Although there are some delays and errors between real data and identified data, the obtained models of the flight dynamics closely estimate the true FWMAV response.

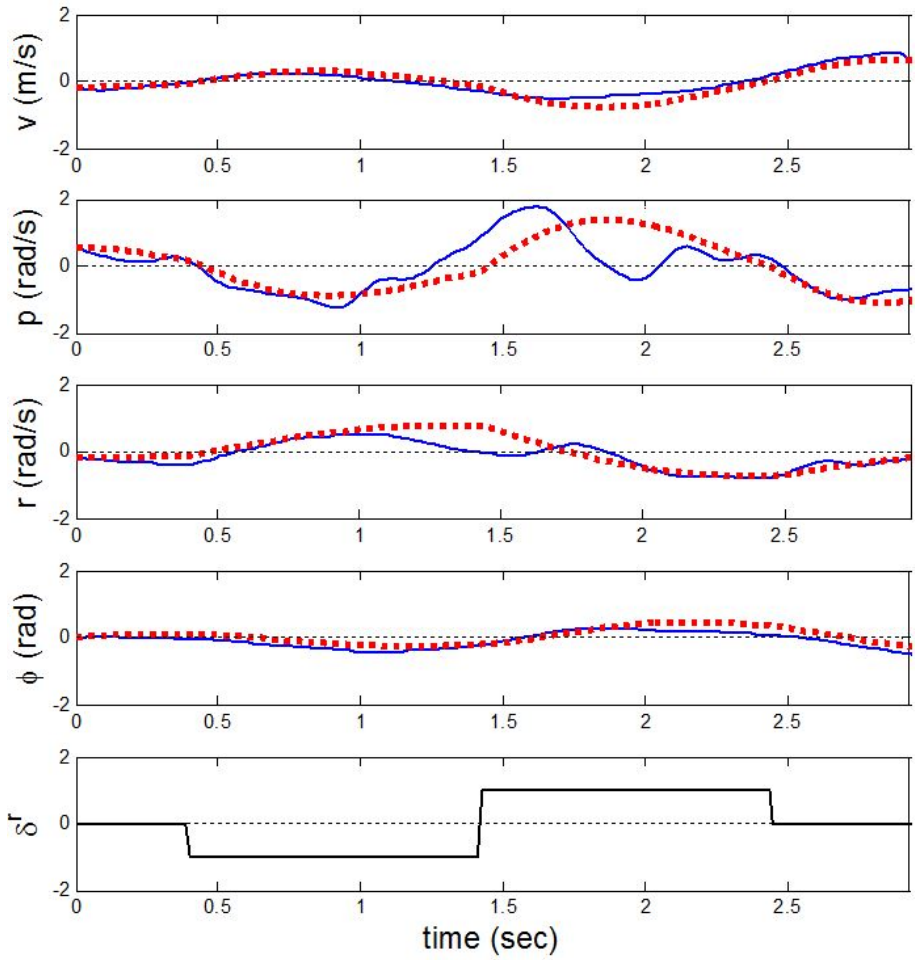

Figure 4.3: Time domain validation results of the lateral dynamics

$$\Delta x_{k+1}^{Lat} = G^{Lat} \Delta x_k + H^{Lat} \Delta u_k^T \tag{4.3}$$

$$G^{Lat} = \begin{bmatrix} 0.9888 & -0.0143 & -0.0240 & 0.0648 \\ -0.0638 & 0.9842 & 0.0153 & -0.1946 \\ 0.0495 & 0.0109 & 0.9949 & 0.0405 \\ 0.0023 & 0.0193 & 0.0094 & 0.9745 \end{bmatrix}, \quad H^{Lat} = \begin{bmatrix} -0.0124 \\ 0.0364 \\ -0.0206 \\ 0.0023 \end{bmatrix}$$

$$\Delta \dot{x}^{Lat} = A^{Lat} \Delta x + B^{Lat} \Delta u^T \tag{4.4}$$

$$A^{Lat} = \begin{bmatrix} -0.6994 & -0.9401 & -1.5250 & 4.0610 \\ -4.0470 & -0.9087 & 0.9739 & -12.290 \\ 3.1400 & 0.6861 & -0.2963 & 2.5330 \\ 0.1727 & 1.2290 & 0.5896 & -1.5080 \end{bmatrix}, \quad B^{Lat} = \begin{bmatrix} -0.7804 \\ 2.2910 \\ -1.2870 \\ 0.1273 \end{bmatrix}$$

Table 4.2: Details of the lateral dynamics

Discrete-time eigenvalue	Continuous-time eigenvalue	Damping	Frequency
0.9827 + 0.0198i	-1.08+1.26i	0.651	1.66
0.9827 - 0.0198i	-1.08-1.26i	0.651	1.66
0.9886 + 0.0533i	-0.626+3.37i	0.183	3.43
0.9886 - 0.0533i	-0.626-3.37i	0.183	3.43

Using linear estimator expressed by (3.4), the system and control matrix in the lateral model can be approximated. The resulting of discrete time model is summarized by the matrices in (4.3) and continuous model converted from the obtained discrete models is also described by the matrices in (4.4).

Eigenvalue decomposition of the system matrix A^{Lat} reveals the modes of lateral dynamics. In general, lateral motion of an fixed-wing aircraft disturbed from its equilibrium flight condition is characterized by three modes, but they are a lot more complicated than the longitudinal case. We see that one mode is simply the damping of rolling motion. This motion is called the roll mode. The second motion is a nonoscillatory divergent motion that can occur when directional stability is large and lateral stability is small; it is called the spiral mode. The third motion is a coupled lateral-directional oscillation that can be quite objectionable to pilots and passengers; it is called the dutch roll mode. On the other hand, the lateral motion of the FWMAV has two pairs of complex conjugate poles. One is $-1.08 \pm 1.26i$ with a damping ratio of 0.651 and natural frequency of 1.66rad/s and the other is $-0.626 \pm 3.37i$ with a damping ratio of 0.183 and natural frequency of 3.43rad/s. The controllability matrix $P = [B \;\; AB \;\; A^2B \;\; A^3B]^{Lat}$ has rank 4. So the linear time-invariant system is controllable. The details of the lateral dynamics are summarized in Table 4.2. Figure 4.4 also shows pole-zero map and bode diagram of lateral dynamics.

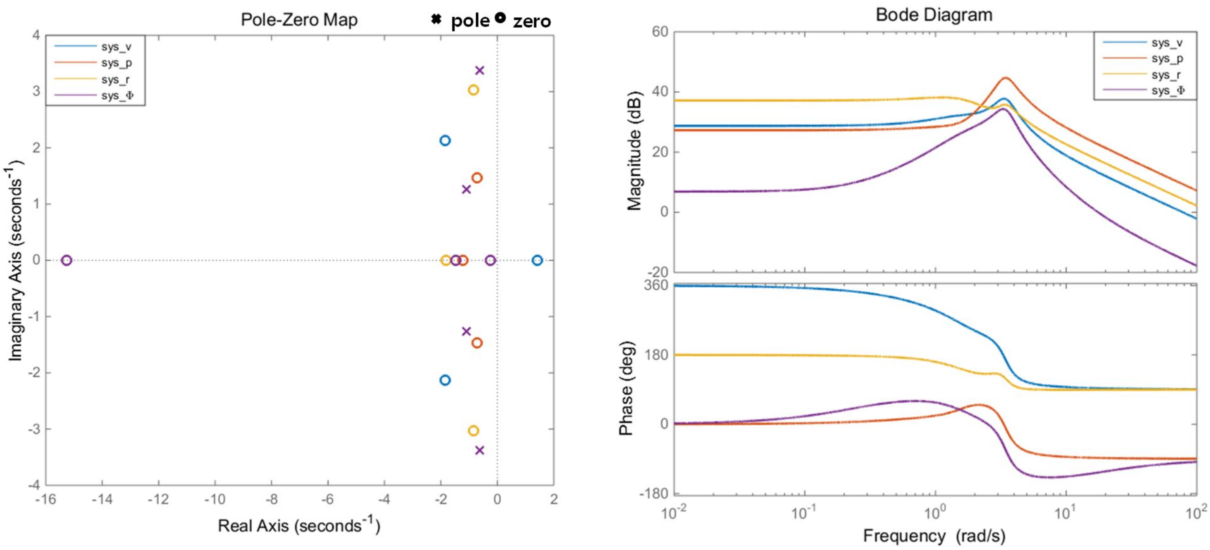

Figure 4.4: Pole-zero map and bode diagram of lateral dynamics

4.3 SVR

An offline trained model is adjusted to follow the FWMAV dynamics and the input-output data sets which are the same with linear estimator case (longitudinal dynamics-identification: 4×2156, verification:4×269, lateral dynamics-identification: 4×269, verification: 4×269) are used for the offline training of the SVR as mentioned in sections 3.5.

The Gaussian radial basis function (GRBF) $K(X_i, X_j) = exp(-(X_i - X_j)^T (X_i - X_j)/\sigma^2)$ which is a popular kernel function used in various kernelized learning algorithms is chosen for (3.13) and σ is a design parameter which is considered based on a validation data set with the goal to achieve a prediction performance. As mentioned earlier, the input set for the SVR consists of the current control input and state variables, and the SVR output is the one-step ahead states. Fig 4.5 shows results of SVR algorithm with results of linear estimator, which accurately produces the FWMAV state variables than linear estimator.

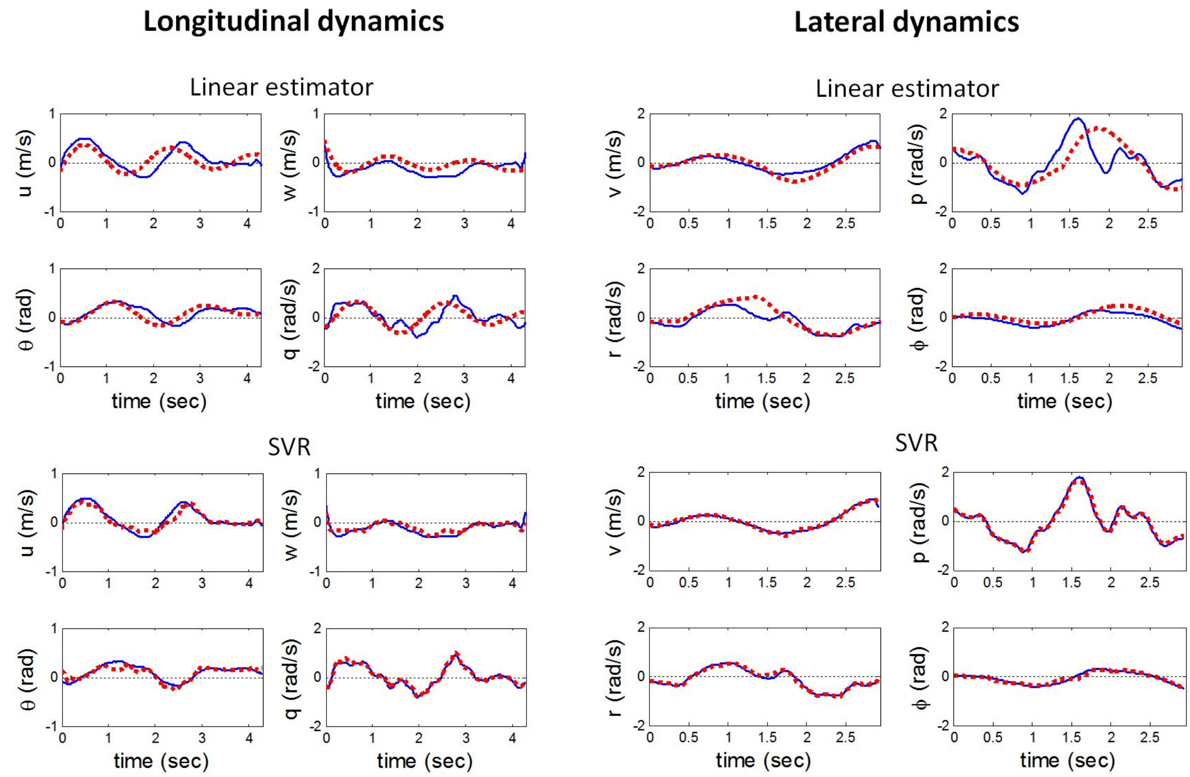

Figure 4.5: Comparison results of the identified model, linear estimator (top) and SVR (down)

5 Controller design

This chapter is organized as follows; Section 5.1 shows responses of feedforward control to the obtained model. Section 5.2 explains pole placement reference tracking control for the discrete-time linear system. Section 5.3 also introduces linear quadratic tracking control for the same system.

5.1 Feedforward control

To determine the overall steady-state values of the FWMAV for maintaining a flight altitude, feedforward control applies to the obtained model. The motion of the model represented (4.2) is simulated for the percentage of flapping motor output between 70 and 100 percent in 5 percent increase. For each trajectory, the flight path is also drawn. The initial conditions are 0.39m/s body velocity, 50 degree pitch angle and 1.5m altitude.

Fig.5.1 shows responses of feedforward control. All of the state trajectories have some oscillatory motions because there is a pair of complex conjugate poles at the longitudinal dynamics. Especially, the 80 percentage of flapping motor output is the specific value to keep an altitude. Table 5.1 shows the transient response specification of the FWMAV and the steady-state values of maintaining an altitude. Settling time of each state is about between 16 and 19 (sec) and it takes so long time to converge towards the steady-state values due to low damping ratio.

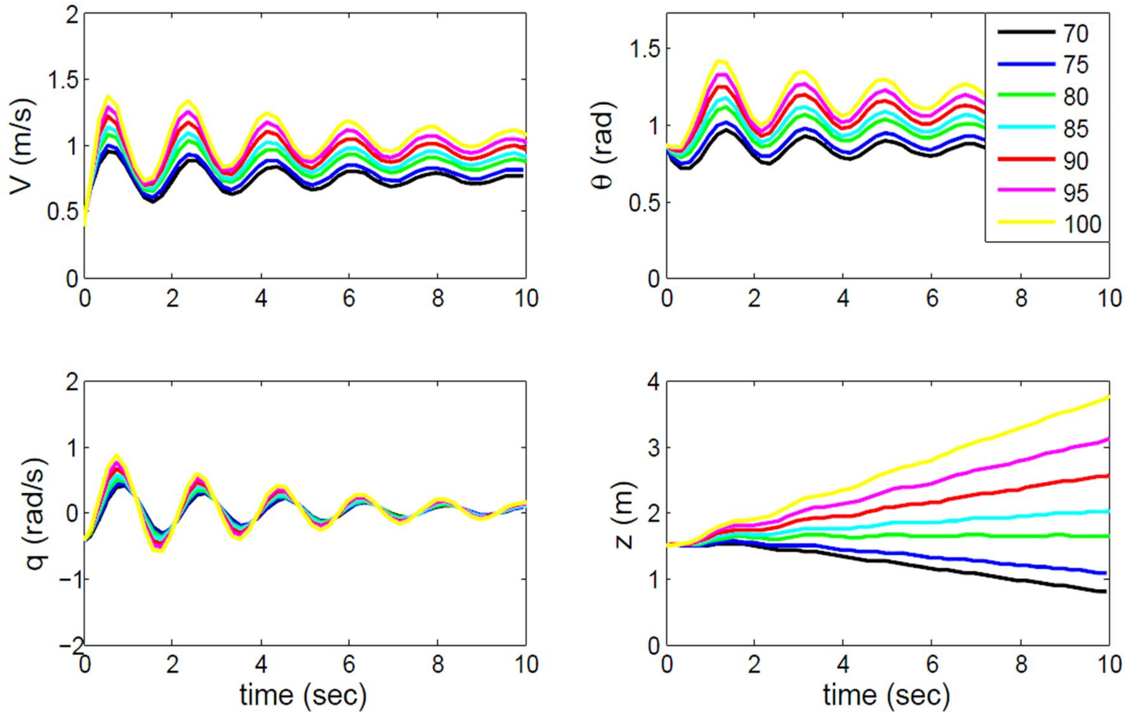

Figure 5.1: Response results of a feedforward control

Table 5.1: Specifications of steady states

	u	v	θ	q
Settling time (sec)	18.7	16.8	16.6	18.1
Steady-state value	0.48	-0.7	0.97	0

5.2 Pole placement reference tracking control

In our problem, the input signal to control pitch angle for the FWMAV is computed based on the reference tracking controller through pole placement to improve convergence speed given by

$$
\begin{aligned}
x_{k+1} &= Gx_k + Hu_k, \;\; x_k = [u_k \;\; w_k \;\; \theta_k \;\; q_k]^T, \;\; u_k = \delta_k^f && (5.1)\\
y_{k+1} &= Cx_k && (5.2)\\
u_k &= -Kx_k + r_{ss} && (5.3)\\
x_{ss} &= N_x r_{ss}, \;\; u_{ss} = N_u r_{ss} && (5.4)
\end{aligned}
$$

where $C = [0 \;\; 0 \;\; 1 \;\; 0]$, x_{ss} is steady-state value, r_{ss} stands for a reference input and K is a 1×4 constant matrix. Substituting (5.4) into (5.1), (5.2) and arranging,

$$
(G - I)N_x + HN_u = 0
$$

$$
CN_x = 1
$$

$$
\begin{bmatrix} N_x \\ N_u \end{bmatrix} = \begin{bmatrix} G - I & H \\ C & 0 \end{bmatrix}^{-1} \begin{bmatrix} 0 \\ 1 \end{bmatrix}
$$

$$
\begin{aligned}
u_k &= u_{ss} - K(x_k - x_{ss}) \\
&= -Kx_k + (N_u + KN_x)r_{ss} && (5.5)
\end{aligned}
$$

Then, the equation of the state-feedback system becomes

$$
x_{k+1} = (G - HK)x_k + H(N_u + KN_x)r_{ss}
$$

Including additional input to control altitude in (5.5)

$$
u_k^* = u_k + K_p(z_{ref} - z_k) + K_d(\dot{z_{ref}} - \dot{z_k}) \tag{5.6}
$$

where K_p is a proportional gain, K_d is a derivative gain and z_{ref} is a reference altitude.

5.3 Linear quadratic tracking control

Some problems where the system dynamics are described by linear differential equations and the cost is described by a quadratic function with operating a dynamic system at minimum cost is called the LQ problem. One of the main results in the theory is a linear-quadratic regulator (LQR) which is a feedback controller and the LQR tracking problem is a deformation on the LQR problem which provides a way to track a reference trajectory for a linear system model. For a discrete-time LTI system of the FWMAV described by

$$x_{k+1} = Gx_k + Hu_k, \;\; x_k = [u_k \quad w_k \quad \theta_k \quad q_k]^T, \;\; u_k = \delta_k^f \tag{5.7}$$

with a performance index and restrictions defined as

$$J = \frac{1}{2}(Cx_N - r_N)^T P(Cx_N - r_N) + \frac{1}{2}\sum_{k=1}^{N-1}[(Cx_k - r_k)^T Q(Cx_k - r_k) + u_k^T Ru_k] \tag{5.8}$$

$$R > 0, P \geq 0, Q \geq 0$$

where $C = [0 \;\; 0 \;\; 1 \;\; 0]$, the optimal control sequence minimizing the performance index (5.8) is given by

$$u_k = -K_k x_k + K_k^v v_{k+1} \tag{5.9}$$

where K_k, K_k^v and S_k, v_k is found iteratively backwards in time by the Riccati equation as follows

$$\begin{aligned}
K_k &= (H^T S_{k+1} H + R)^{-1} H^T S_{k+1} G \\
K_k^v &= (H^T S_{k+1} B)^{-1} H^T \\
S_k &= G^T S_{k+1}(G - HK_k) + C^T QC \\
v_k &= (G - HK_k)^T v_{k+1} + C^T Q r_k
\end{aligned}$$

from terminal condition $S_N = C^T PC$ and $v_N = C^T P r_N$.

6 Results

This chapter is organized as follows; Section 6.1 shows simulation results of the feedforward control, pole-placement reference tracking control and linear quadratic tracking control. Section 6.2 shows experimental results of the FWMAV for maintaining an altitude.

6.1 Simulation results

Fig 6.1 shows results of altitude control described in section 5 for the obtained model (4.1). The black line, blue line and green line mean the consequences of applying feedforward control, pole placement reference tracking control and LQ-tracking control, and the red line is reference values for keeping a flight altitude.

We can see that the black line has oscillation motion during whole time history, but the others only have once or twice vibration motion at an initial phase. In addition, the black line has slow convergence speed than others to reach the reference values. These results are obvious because the system which uses the feedforward control responds to its control signal in a pre-defined way without additional information. Fig 6.2 shows results of flight state of the FWMAV following the reference altitude 2m as seen from side and XZ plane view.

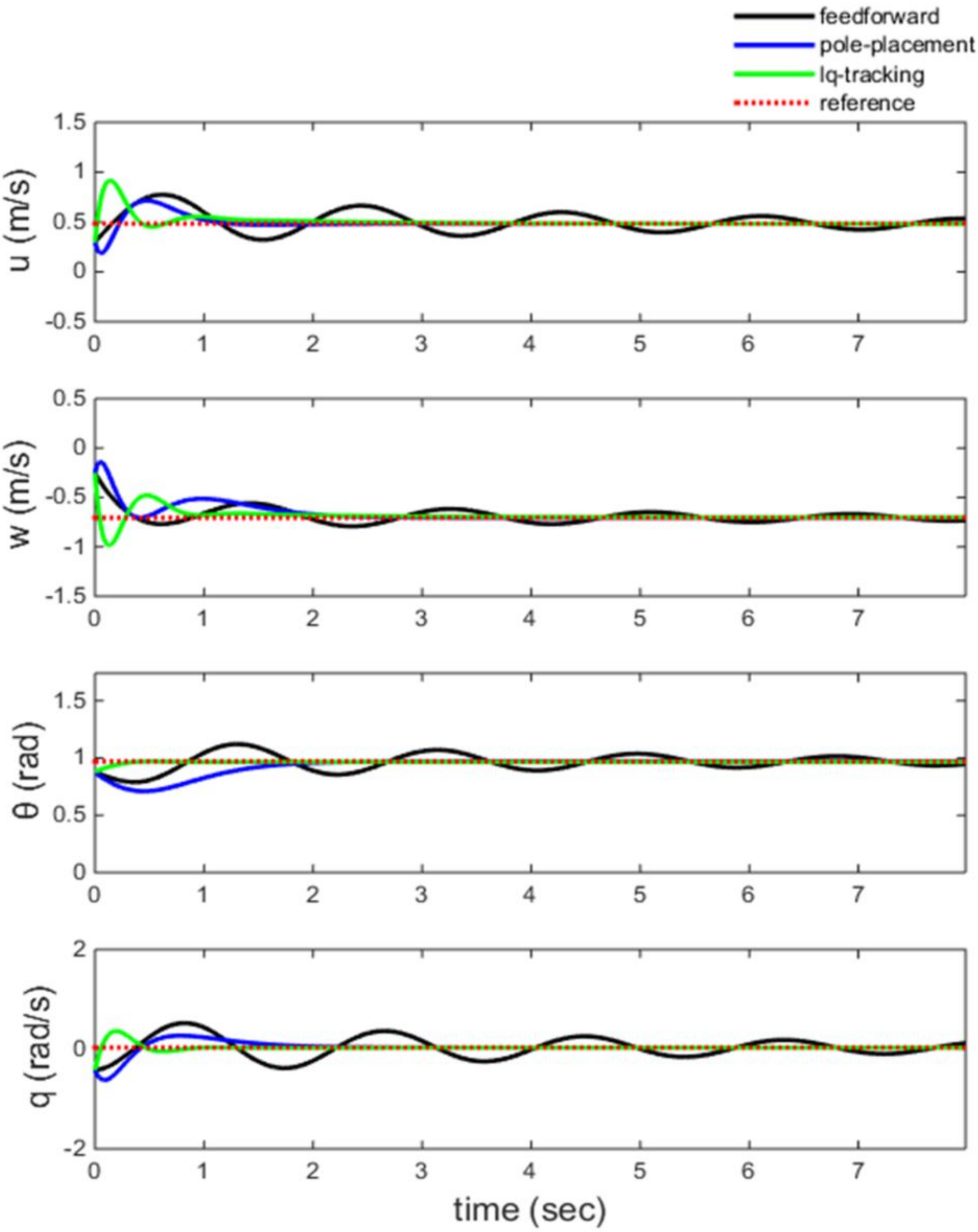

Figure 6.1: Changes of the state variables in simulation environment

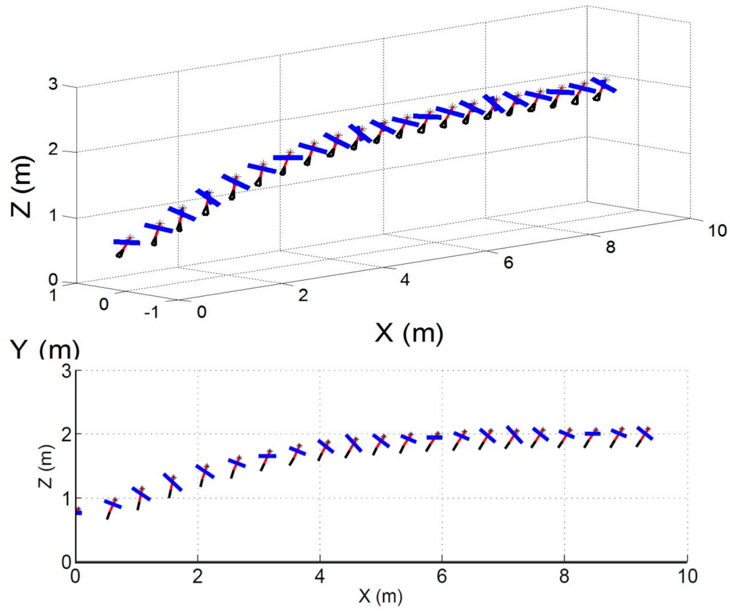

Figure 6.2: Flight state of the FWMAV. Side view (top) and XZ plane view (down)

6.2 Experimental results

The hardware setup for flight experiment appears in Fig 6.3. First, A motion capture system composed of 8 vicon cameras estimates the position (x, y, z) and attitude (ϕ, θ, ψ) of the FWMAV. In the ground station, those data recorded from vicon cameras is transmitted to a ground station computer through Ethernet networks. Then, motion capture software calculates the velocity (u, v, w) and angular velocity (p, q, r) in body coordinates, respectively. Afterwards, control software computes the control input which activates the flapping motor to maintain a flight altitude with running at 70Hz using estimated state variables. Control flows are represented in Fig 6.4.

Fig 6.5 shows experimental results of maintaining an altitude using pole placement reference tracking controller. 3 test results are plotted on the graph with the reference values which correspond to the desired values to keep a flight height in simulation environment. Although the state variables controlled by controller in simulation environment exactly follow the reference values, the state variables in actual experiment have some noticeable deviations from set values in flight.

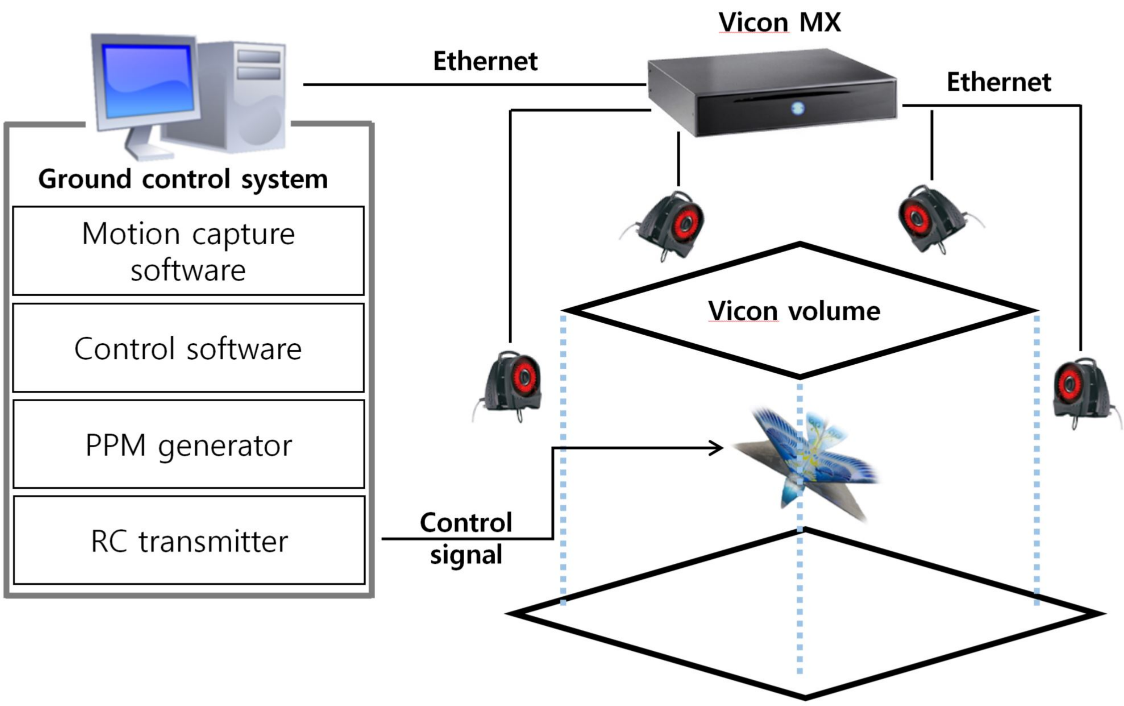

Figure 6.3: Configuration for flight experiment

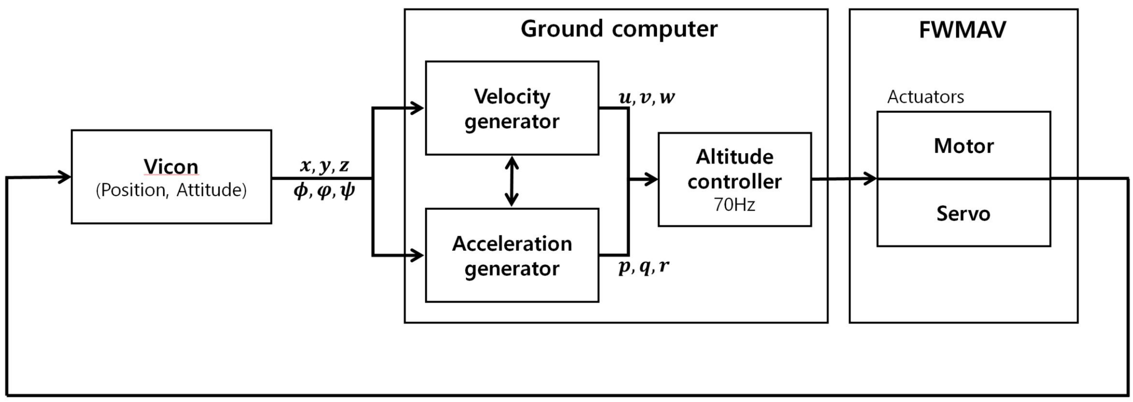

Figure 6.4: Configuration of the control system

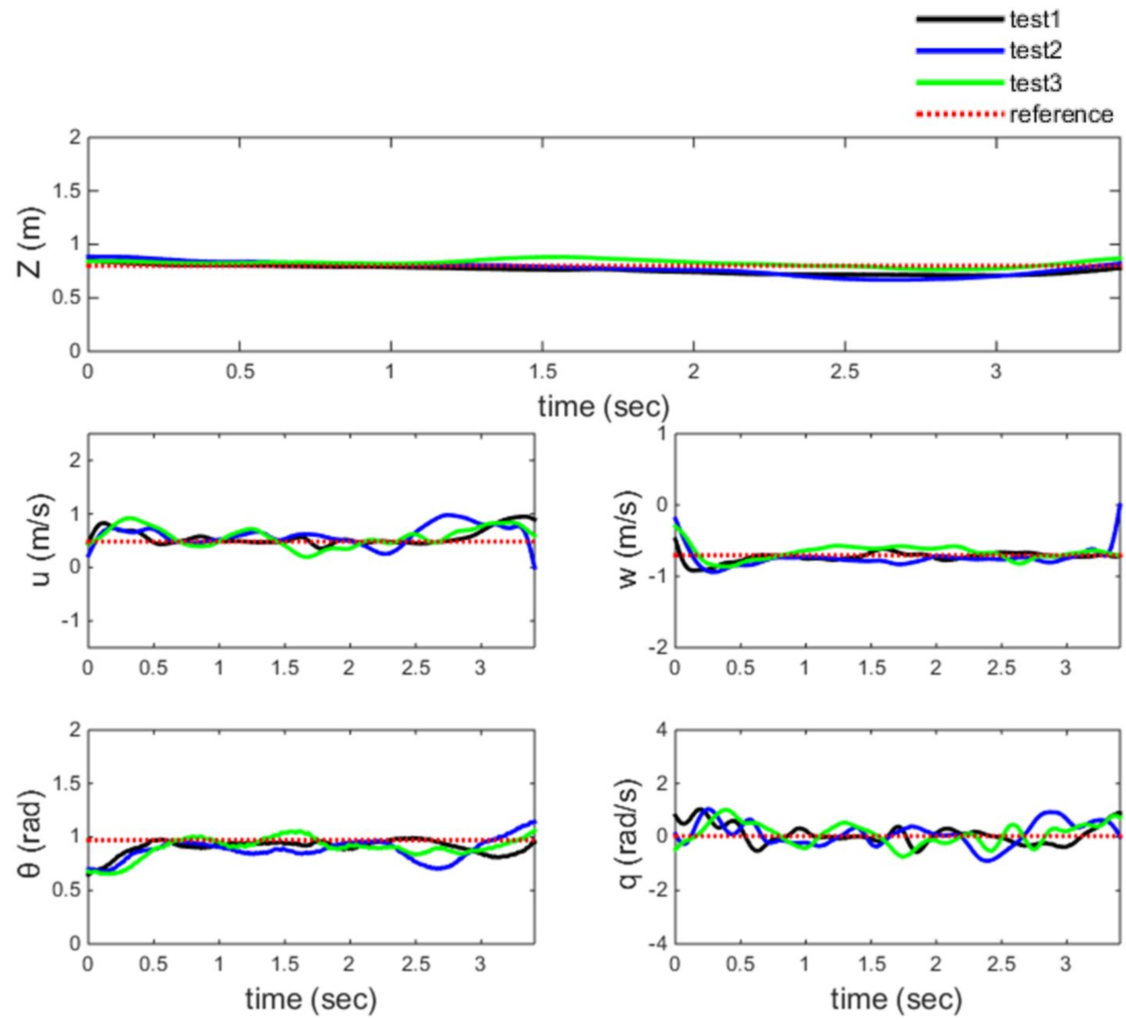

Figure 6.5: Changes of the state variables in experiment

7

Conclusion

In this thesis, we conducted system identification of the longitudinal and lateral dynamics of the FWMAV using time domain techniques in order to apply linear control methods. To gather input-output data sets from flight test, we constructed a control experiment setup for a MAV in an indoor environment using a motion capture system. The necessary assumptions are used to simplify model structures. We could compare the two methods, one is linear estimator and the other is SVR algorithm, and know that the latter way accurately produces the true FWMAV responses better than the former way. But SVR algorithm does not provide system models for analyzing dynamic characteristic. Therefore, we could obtain discrete time LTI models of the FWMAV using linear estimator. It is also suited for flight control as baseline models. After dynamic characteristics of the FWMAV are checked through matrix analysis, the acquired model is used to design feedback controllers such as pole placement reference tracking control and linear quadratic control for maintaining altitude. To verify those controllers, the simulation is performed and the results showed that linear controllers give a good tracking performance. The experimental results also show satisfactory control performance. Our future work is to research autonomous flight of the FWMAV to be used in reconnaissance and surveillance missions.

References

[1] Baek, Stanley S., and Ronald S. Fearing. "Flight forces and altitude regulation of 12 gram i-bird." Biomedical Robotics and Biomechatronics (BioRob), 2010 3rd IEEE RAS and EMBS International Conference on. IEEE, 2010.

[2] Baek, Stanley S., Fernando L. Garcia Bermudez, and Ronald S. Fearing. "Flight control for target seeking by 13 gram ornithopter." Intelligent Robots and Systems (IROS), 2011 IEEE/RSJ International Conference on. IEEE, 2011.

[3] De Croon, G. C. H. E., et al. "Design, aerodynamics, and vision-based control of the DelFly." International Journal of Micro Air Vehicles 1.2 (2009): 71-97.

[4] De Croon, G. C. H. E., et al. "The appearance variation cue for obstacle avoidance." Robotics, IEEE Transactions on 28.2 (2012): 529-534.

[5] Jung, Han-Kyo, et al. "Analysis and Fabrication of Unconventional Flapping Wing Air Vehicles." International Journal of Micro Air Vehicles 7.1 (2015): 71-88.

[6] Cheol Park, Hoon, Eko Priamadi, and Quang-Tri Truong. "Effect of flapping-wing kinematics on force generation." International Journal of Intelligent Unmanned Systems 1.3 (2013): 245-255.

[7] Whitney, J. P., and R. J. Wood. "Aeromechanics of passive rotation in flapping flight." Journal of Fluid Mechanics 660 (2010): 197-220.

[8] Duan, Hongjun, and Qingwei Li. "Dynamic model and attitude control of flapping wing micro aerial vehicle." Robotics and Biomimetics (ROBIO), 2009 IEEE International Conference on. IEEE, 2009.

[9] Fuller, Sawyer B., et al. "Estimating attitude and wind velocity using biomimetic sensors on a microrobotic bee." Robotics and Automation (ICRA), 2013 IEEE International Conference on. IEEE, 2013.

[10] Ljung, Lennart. System identification. Birkhäuser Boston, 1998.

[11] Tischler, Mark B., and Robert K. Remple. "Aircraft and rotorcraft system identification." AIAA Education Series. American Institute of Aeronautics and Astronautics, New York (2006).

[12] Dorobantu, Andrei, et al. "Frequency domain system identification for a small, low-cost, fixed-wing uav." Proceedings of the 2011 AIAA Guidance, Navigation, and Control Conference. 2011.

[13] Dorobantu, Andrei, et al. "System identification for small, low-cost, fixed-wing unmanned aircraft." Journal of Aircraft 50.4 (2013): 1117-1130.

[14] Schafroth, D., et al. "Modeling, system identification and robust control of a coaxial micro helicopter." Control Engineering Practice 18.7 (2010): 700-711.

[15] Gremillion, Gregory, and J. Sean Humbert. "System identification of a quadrotor micro air vehicle." AIAA Conference on Atmospheric Flight Mechanics. 2010.

[16] Smola, Alex J., and Bernhard Schölkopf. "A tutorial on support vector regression." Statistics and computing 14.3 (2004): 199-222.

[17] Vapnik, Vladimir. The nature of statistical learning theory. Springer Science-Business Media, 2013.

[18] Cherkassky, Vladimir, and Yunqian Ma. "Practical selection of SVM parameters and noise estimation for SVM regression." Neural networks 17.1 (2004): 113-126.

국 문 초 록

본 논문에서는 기록된 비행 데이터를 이용해 날갯짓 비행체의 동적 모델을 예측하는 기법인 시스템 식별에 초점을 두고 있다. 고정익 비행체와 회전익 비행체와는 달리 날갯짓 비행체의 수학적 모델은 비선형성이 강하고 상태변수들이 서로 복잡하게 연관되어 있는 것이 특징이다. 따라서 문제를 단순화 시키기 위해 날갯짓 비행체의 종방향과 횡방향 모델을 이산시간 선형시스템이라 가정해 문제에 접근하였다. 또한 실내환경에서의 GPS 시스템인 모션 캡쳐 시스템을 활용해 날갯짓 비행체를 대상으로 제어입력과 비행 데이터를 수집할 수 있는 실험장비를 구축하였다. 이를 이용해 수 차례 실내비행을 수행함으로써 신뢰성을 가진 풍부한 양의 데이터를 수집할 수 있었다. 그 후 linear estimator와 support vector regression (SVR)을 적용시켜 날갯짓 비행체의 동적 모델을 예측하고 시간 영역에서의 데이터를 바탕으로 모델의 정확성을 검증하였다. 종방향과 횡방향 모델의 행렬 분석을 통해 각각의 모델이 가지고 있는 동적 특성을 확인하였으며 획득한 모델을 이용해 날갯짓 비행체의 비행 고도를 제어할 수 있는 선형 되먹임 제어기를 설계하였다. 또한 시뮬레이션과 실험을 통해 설계한 제어기를 적용시켜 보았으며 그 성능을 확인 할 수 있었다.

주요어 : 시스템 식별, 종방향 및 횡방향 모델, 날갯짓 비행체, 선형 관측기, 서포트 벡터 회귀

학번 : 2013-23067